Analytical Small-Signal Transfer Functions for Phase Shift Modulated Dual Active Bridge Converters Using Phasor Transformation

Weijian Han
School of Automation
Northwestern Polytechnical University
Xi'an, China
hanweijian@mail.nwpu.edu.cn

Luca Corradini
Department of Information Engineering
University of Padova
Padova, Italy
luca.corradini@dei.unipd.it

***Abstract*—This paper derives the analytical small-signal transfer functions for phase shift modulated dual active bridge (DAB) converters using phasor transformation approach. Transfer functions in closed-form are derived for both voltage source and resistive load, which shows significant simplification compared with the generalized average models. Based on the results obtained, the inherent resonant property near the switching frequency is disclosed which contributes to stable control loop design. The theoretical analysis is verified via computer simulation and experimental test.**

***Index Terms*—dual active bridge, small-signal, transfer function, control, phase shift**

I. Introduction

Dual active bridge (DAB) converters are widely used in the applications requiring bidirectional power transmission, such as dc micro grid, electric vehicles and uninterruptible power supplies. Either output current or voltage needs to be dynamically regulated through a feedback control loop. For the stable closed-loop controller design, a small-signal model is the indispensable tool providing the basic knowledge of dynamic behaviors.

A continuous-time model is usually preferred because it offers more physical insight and facilitates control design. According to whether the dynamics of inductor current is considered, there are two types of models: full-order [1] and reduced-order [2] [3] models. The former ones are usually based on the generalized average modeling (GAM) approach [4] which represents the state variables using its Fourier series and are more accurate for the dynamics prediction. However, the GAM-based small-signal models are expressed in the form of state-space equations and it is difficult to derive *analytical* transfer functions due to the complicated matrix inversion calculation, especially when more Fourier items of inductor current are included to achieve better accuracy.

Analytical transfer functions, especially the control-to-output one, are more desired to perform control loop analysis and design, particularly for a DAB converter operated in wide input/output voltage condition. The objective of this paper is to derive the analytical control-to-output transfer functions for DAB converters with voltage source load and resistive load. Furthermore, the derived analytical results confirm the resonance phenomenon of small-signal behavior around switching frequency and provide effective guidance for a reliable control loop design. Different from the previous GAM-based modeling method, in this paper, phasor transformation technique [5] is employed to formulate a full-order small-signal model. Such approach provides explicit and simple equations, and has been used for the analysis and modeling of series resonant dc-dc converters [5] [6] [7].

The topology of a DAB converter is shown in Fig. 1a which is composed of an ac link and two voltage-source full-bridge circuits with dc bus voltage V_g and V_o, respectively. The ac link consists of an inductor L and a high-frequency transformer with negligible magnetizing current, and the parasitic resistant is represented as R_{par}. The load can be either a voltage source (battery) or a resistor. In the following analysis, transformer turns ratio n is assumed to 1 and phase shift modulation is here considered in which duty cycles of bridge output voltages v_A and v_B are fixed to 50% and phase shift ϕ between them is adjusted for power control as shown in Fig. 1b.

II. Phasor Transformed Circuit

The first step of small-signal modeling is to derive the phasor transformed equivalent circuit, in which only the fundamental components of inductor current $i_L(t)$ and bridge output voltages $v_A(t)$, $v_B(t)$ are considered. According to the circuit theory, sinusoidal signals with the same frequency can be represented in phasor form

$$x(t) = Re[\vec{x}(t)e^{jw_s t}]. \tag{1}$$

where, $\vec{x}(t)$ indicates the complex time-varying variable with amplitude for representation.

According to [5] [7], all the ac quantities in Fig. 1a can be transformed into phasor form, and hence the phasor transformed equivalent circuit of the DAB converter is shown in Fig. 2. Notice that, inductor current $\vec{i}_{L1}(t)$ and bridge

Weijian Han is sponsored by China Scholarship Council, 201606290074.

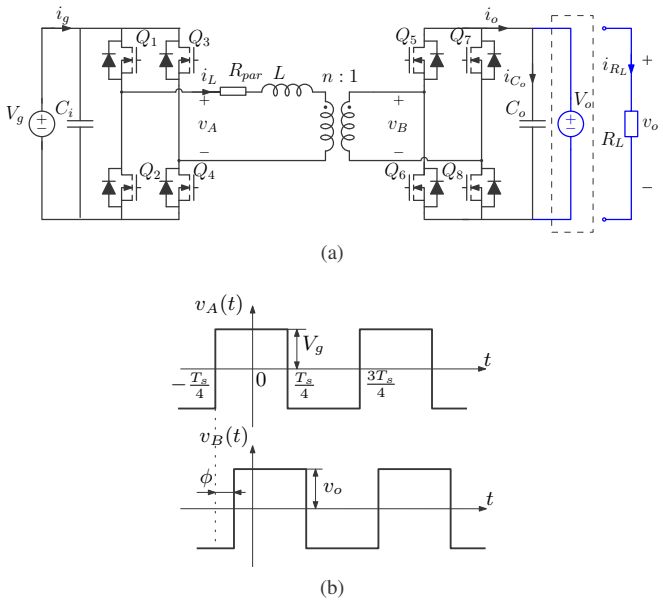

Fig. 1. (a) Topology of dual active bridge dc-dc converter with voltage source load and resistive load, (b) bridge output voltages with phase shift modulation.

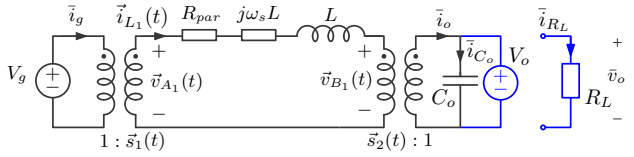

Fig. 2. Phasor transformed circuit of dual active bridge converters.

output voltages $\vec{v}_{A1}(t)$ and $\vec{v}_{B1}(t)$ are expressed in phasor form (subscript 1 indicates the fundamental component). The inductor is represented as a complex resistance $j\omega_s L$ in series with an ideal inductance L, where $\omega_s = 2\pi f_s$ is the switching angular frequency. The two switch networks are substituted by two time-varying transformers with turns ratio $\vec{s}_1(t)$ and $\vec{s}_2(t)$ in phasor form. The average output voltage (for resistive load) and current are respectively denoted as $\bar{v}_o$ and $\bar{i}_o$.

The dc and ac quantities are linked by the equivalent transformers and the relationship between them are

$$\begin{cases} \vec{v}_{A1}(t) = \vec{s_1}(t) \cdot \bar{v}_g \\ \bar{i}_g(t) = \dfrac{1}{2} Re[\vec{s_1}(t)^* \cdot \vec{i}_L(t)] \end{cases} \tag{2}$$

$$\begin{cases} \vec{v}_{B1}(t) = \vec{s_2}(t) \cdot \bar{v}_o \\ \bar{i}_o(t) = \dfrac{1}{2} Re[\vec{s_2}(t)^* \cdot \vec{i}_L(t)] \end{cases} \tag{3}$$

III. Small-signal Models

A. Voltage Source Load

A DAB converter with voltage source load corresponds to applications that the converter charges battery packs or injects power into dc-grid. In this case, the input and output voltages can be regarded as constant. The control input is phase shift ϕ while the output is output current $\bar{i}_o$. Thus, the output capacitor C_o is bypassed and the current flows through C_o ($\bar{i}_{C_o}$) equals to zero.

According to the waveform of bridge output voltages $v_A(t)$, $v_B(t)$ in Fig. 1b, the fundamental component $v_{A1}(t)$, $v_{B1}(t)$ can be expressed as

$$\begin{aligned} v_{A1}(t) &= \frac{4}{\pi} V_g \cos(\omega_s t) \\ v_{B1}(t) &= \frac{4}{\pi} V_o \cos(\omega_s t - \phi). \end{aligned} \tag{4}$$

Then, the time-varying turn ratios of the equivalent transformers, $s_1(t)$ and $s_2(t)$, are represented as

$$\begin{aligned} s_1(t) &= \frac{v_{A1}(t)}{V_g} = \frac{4}{\pi} \cos(\omega_s t) \\ s_2(t) &= \frac{v_{B1}(t)}{V_o} = \frac{4}{\pi} \cos(\omega_s t - \phi), \end{aligned} \tag{5}$$

The turn ratios are transformed into phasor form as $\vec{s}_1(t) = \frac{\pi}{4}$ and $\vec{s}_2(t) = \frac{\pi}{4} e^{-j\phi}$. Thus, the bridge output voltages in phasor domain are $\vec{v}_{A1}(t) = \vec{s}_1(t) \cdot V_g$ and $\vec{v}_{B1}(t) = \vec{s}_2(t) \cdot V_o$.

According to Fig. 2, the inductor current is expressed as

$$\vec{i}_{L1}(t) = \frac{\vec{v}_{A1}(t) - \vec{v}_{B1}(t)}{Z} \tag{6}$$

where $Z = R_{par} + j\omega_s L + sL$ is the impedance of ac link and s is the differential operator. Substituting the expressions of $\vec{s}_2(t)$ and $\vec{i}_{L1}(t)$ into (2), the average output current can be derived as

$$\bar{i}_o(t) = \left(\frac{2}{\pi}\right)^2 \left(\frac{V_g e^{j\phi} - V_o}{Z} + \frac{V_g e^{-j\phi} - V_o}{Z^*} \right), \tag{7}$$

where $Z^* = R_{par} - j\omega_s L + sL$. The steady-state output current I_o can be derived as

$$I_o = V_g \frac{8}{\pi^2} \frac{(R_{par} \cos\Phi + \omega_s L \sin\Phi) - V_o R_{par}}{(R_{par}^2 + \omega_s^2 L^2)}, \tag{8}$$

where I_o and Φ indicate the steady-state value. Note that int the steady state, the differential operator s of Z is zero.

Linearizing equation (7), the control-to-output transfer function $G_{i_o\phi}(s)$ is

$$G_{i_o\phi}(s) = \frac{\hat{i}_o}{\hat{\phi}} = V_g \frac{8}{\pi^2} \frac{-\sin\Phi L s + \omega_s L \cos\Phi - R_{par} \sin\Phi}{L^2 s^2 + 2R_{par} L s + R_{par}^2 + \omega_s^2 L^2}. \tag{9}$$

B. Resistive Load

For a DAB converter connected with a resistive load, the control input is phase shift ϕ while the output is voltage $\bar{v}_o$ which is time-varying. Therefore, in this case, $\bar{i}_{C_o} \neq 0$. With respect to the small-signal derivation, firstly, the output current $\bar{i}_o$ is expressed using (2)

$$\bar{i}_o(t) = \left(\frac{2}{\pi}\right)^2 \left(\frac{V_g e^{j\phi} - \bar{v}_o}{Z} + \frac{V_g e^{-j\phi} - \bar{v}_o}{Z^*} \right). \tag{10}$$

On the other hand, according to Fig. 2, in the output side, output current can be represented as

$$\bar{i}_o = C_o \frac{d\bar{v}_o}{dt} + \frac{\bar{v}_o}{R_L}. \tag{11}$$

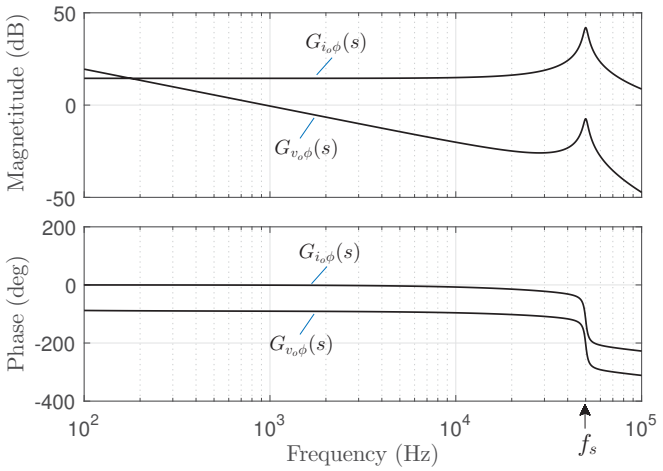

Fig. 3. Amplitude- and phase-frequency curves of $G_{i_o\phi}(s)$ and $G_{v_o\phi}(s)$. $G_{i_o\phi}(s)$: $V_g = 200\,\text{V}$, $V_o = 150\,\text{V}$ and $P_o = 500\,\text{W}$, $G_{v_o\phi}(s)$: $V_g = 200\,\text{V}$, $R_L = 47\,\Omega$ and $P_o = 480\,\text{W}$

From (10) and (11), the steady-state output voltage is deduced as

$$V_o = V_g \frac{8}{\pi^2} \frac{(R_{par}\cos\Phi + \omega_s L \sin\Phi)}{\frac{1}{R_L}(R_{par}^2 + \omega_s^2 L^2) + \frac{8}{\pi^2} R_{par}}. \tag{12}$$

The control-to-output transfer function $G_{v_o\phi}(s)$ can be further derived and shown in (13).

The derived analytical transfer functions (9) and (13) are the main results of this paper, which can be directly used to evaluate small-signal dynamics related to converter parameters (L, R_{par}, etc.) and operating conditions (V_g, ϕ, etc.), and facilitate a closed-loop controller design.

Compared with the GAM approach, small-signal modeling with phasor transformation contributes to easily derive analytical transfer functions. This is particular true when more inductor current harmonics are considered for achieving better accuracy. Using phasor transformation modeling, analytical transfer functions $G_{i_o\phi}(s)$ and $G_{v_o\phi}(s)$ are still achievable by superimposing the contribution of each harmonics. However, for the GAM-based modeling, it is unfeasible to achieve due to the involvement of complicated high-order matrix calculation.

C. Small-Signal Dynamics Analysis

It can be seen from (9), the transfer function $G_{i_o\phi}(s)$ is 2nd order and has a pair of conjugate poles $p_1 = -\frac{R_{par}}{L} + j\omega_s$, $p_2 = -\frac{R_{par}}{L} - j\omega_s$. The damping ratio ξ and nature frequency ω_n are

$$\xi = \frac{R_{par}}{\sqrt{R_{par}^2 + \omega_s^2 L^2}}, \qquad \omega_n = \frac{\sqrt{R_{par}^2 + \omega_s^2 L^2}}{L}. \tag{14}$$

Usually, for a DAB converter, $R_{par} \ll \omega_s L$, hence $\xi \ll 1$ and $\omega_n \approx \omega_s$, which indicates the converter is under damped and there exists a resonant peak in the amplitude-frequency characteristic at resonant frequency $\omega_r = \omega_n\sqrt{1-2\xi^2} \approx \omega_s$. Such conclusion still holds for the 3rd order transfer function $G_{v_o\phi}(s)$. The poles of $G_{v_o\phi}(s)$ can be approximately calculated as p_1, p_2 (the same with $G_{i_o\phi}(s)$) and $p_3 = -\frac{1}{C_o R_L}$. In contrast to $G_{i_o\phi}(s)$, the resonant peak is lower due to the effect of p_3.

Amplitude- and phase-frequency characteristic curves of $G_{i_o\phi}(s)$ and $G_{v_o\phi}(s)$ are respectively shown in Fig. 3 (converter parameters and steady-state conditions are given in section IV). It clearly shows the resonant behavior around switching frequency, which limits the bandwidth of control loop. In order to achieve stable close-loop operation, attention should be paid to preventing the resonant peak from crossing the 0 dB line.

Physical explanation of the resonance phenomenon around switching frequency f_s is that the perturbation at vicinity of f_s introduces low frequency sideband in the bridge output voltage $v_B(t)$, and then results in a strong inductor current response. Such a low frequency current further exerts serious effects on output current or voltage. Fig. 4a shows the PWM carrier waveform of phase shift modulator of both primary and secondary side. It can be seen, when a small-signal perturbation with $f = f_s$ is exerted, the PWM carrier of secondary side is disturbed with frequency f_s and hence a dc component is introduced. With such an effect, the duty cycle of bridge output waveform $v_B(t)$ is not 50% and appears dc component which results in a high bias current, as indicated in Fig. 4b.

IV. Simulation and Experimental Verification

Simulation and experimental results are presented to verify the derived transfer functions and theoretical analysis. Parameters of the DAB converter are $L = 83\,\mu\text{H}$, $R_{par} = 80\,\text{m}\Omega$ and $n = 1$. The value of output capacitance is $C_o = 940\,\mu\text{F}$ and switching frequency is $f_s = 50\,\text{kHz}$.

A. Simulation Verification

Firstly, the proposed analytical small-signal transfer functions are verified by means of PLECS ac sweep analysis. Fig. 5 reports simulated small-signal control-to-output gains and phases with voltage source and resistive load, respectively. The input voltage is $V_g = 200\,\text{V}$. In the voltage source load simulation, V_o is fixed to $150\,\text{V}$ and phase shift $\phi = \frac{\pi}{6}$ leading to output power $P_o = 500\,\text{W}$. In resistive load test, load resistance $R_L = 47\,\Omega$ and phase shift equals to $\frac{\pi}{6}$ with $P_o = 480\,\text{W}$. It can be seen, the simulation results show good consistency with the derived analytical transfer functions (9)

$$G_{v_o\phi}(s) = \frac{\hat{v}_o}{\hat{\phi}} = \frac{V_g\left(\frac{8}{\pi^2}\right)(-sL\sin\Phi + \omega_s L\cos\Phi - R_{par}\sin\Phi)}{C_o L^2 s^3 + (\frac{L^2}{R_L} + 2R_{par}LC_o)s^2 + ((R_{par}^2 + \omega_s^2 L^2)C_o + (2\frac{R_{par}}{R_L} + \frac{8}{\pi^2})L)s + \frac{R_{par}^2+\omega_s^2L^2}{R_L} + \frac{8}{\pi^2}R_{par}} \tag{13}$$

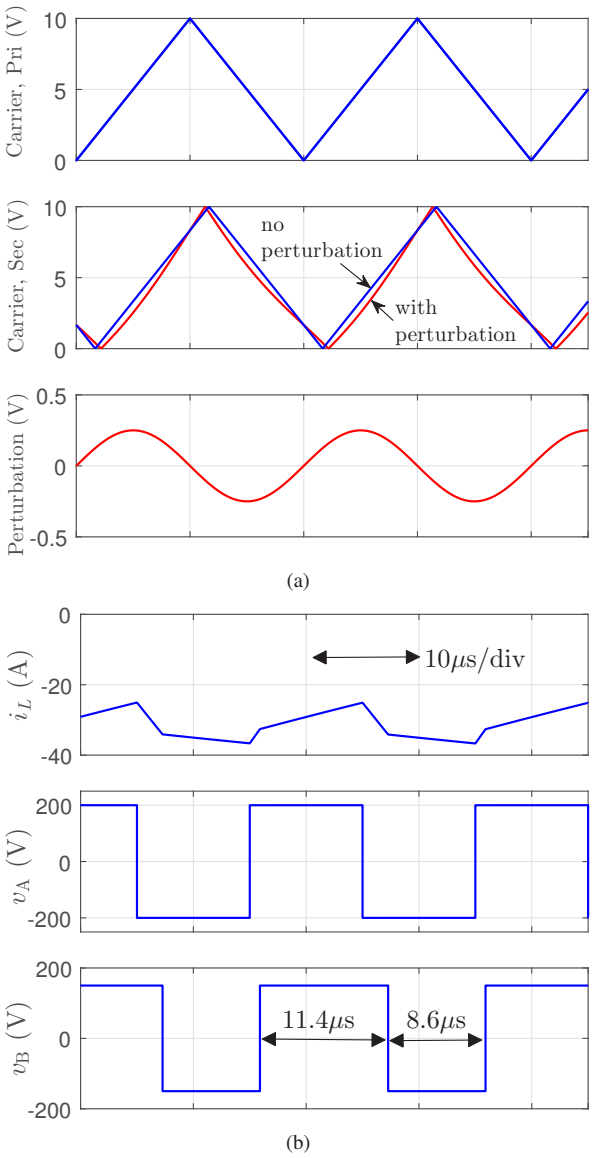

Fig. 4. (a) Carrier waveform of phase shift modulator in primary and secondary side and perturbation signal ($f = f_s$), and (b) inductor current and bridge output voltages waveform under the perturbation.

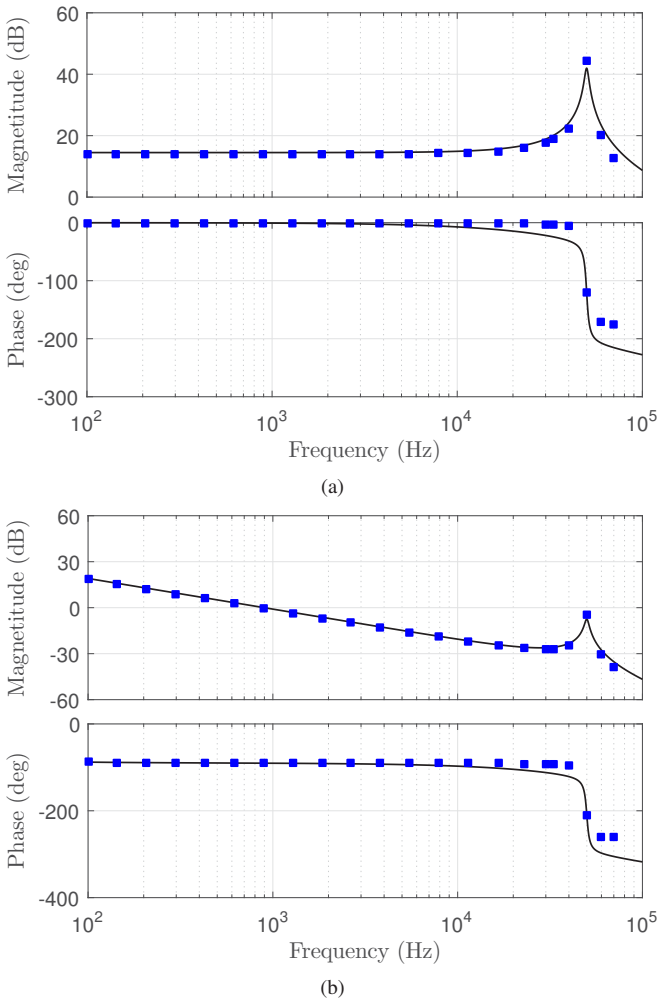

Fig. 5. Simulated frequency response of the DAB converter, (a) with voltage source load, (b) with resistive load.

and (13). The resonant peak near the switching frequency is also verified which confirms the theoretical prediction.

Then, closed-loop simulation is performed to verify the effectiveness of proposed analytical transfer functions in the compensator design. Due to the high ripple in the output current, a 1st-order filter with cutoff frequency 1 kHz is used to smooth the output current. For comparison, closed-loop operation with two proportional-integral (PI) controllers are simulated under voltage source load condition. The integral coefficients in these two PI controller are the same, i.e. $k_i = 1000$, whereas, the proportional coefficient are $k_p = 0.2$ and $k_p = 0.5$, respectively. The bode plot of loop gain $T_{io}(s) = k_p G_{i_o\phi}(s)$ is shown in Fig. 6a. It can be seen, for $k_p = 0.2$ the resonant peak is below 0 dB line with magnitude margin around 6 dB, while in terms of $k_p = 0.5$, the resonant peak crosses the 0 dB line. Fig. 6b and Fig. 6c reports the closed-loop waveforms with a reference output current 3 A. It indicates that, for the PI controller with $k_p = 0.2$ (Fig. 6b), the DAB converter achieves stable operation. In contrast to this, with $k_p = 0.5$ (Fig. 6c), the converter is unstable and a large dc bias can be seen in the inductor current waveform.

Also, closed-loop simulation under the resistive load condition is performed with two proportional (P) controllers. The first one is $k_p = 0.8$ and the bode plot of loop gain $T_{vo}(s) = k_p G_{v_o\phi}(s)$ is indicated in Fig. 7a where the resonant peak is below 0 dB line with magnitude margin 10 dB. The second one is $k_p = 3$, with which the resonant peak crosses the 0 dB line. It can be further confirmed that, when $k_p = 0.8$, all the roots of $1 + T_{vo}(s)$ (the poles of closed-loop transfer function) are in the left half plane. Conversely, for $k_p = 3$, two roots are located in the right half plane. Fig. 7b and Fig. 7c report the closed-loop simulation waveforms with reference output voltage 150 V. The initial output capacitor voltage is set to 150 V. It can be seen, for the controller

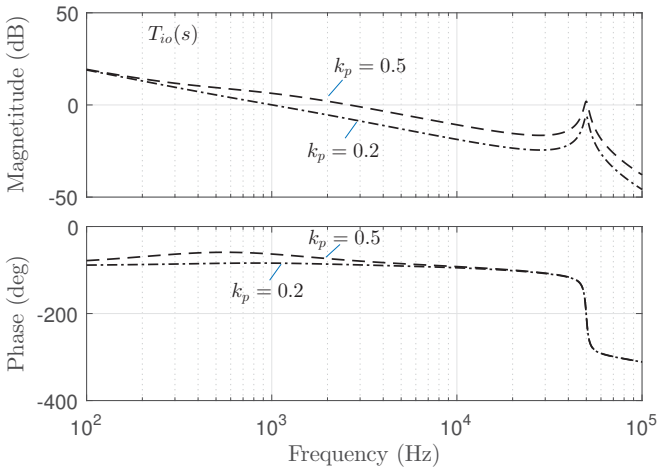

(a)

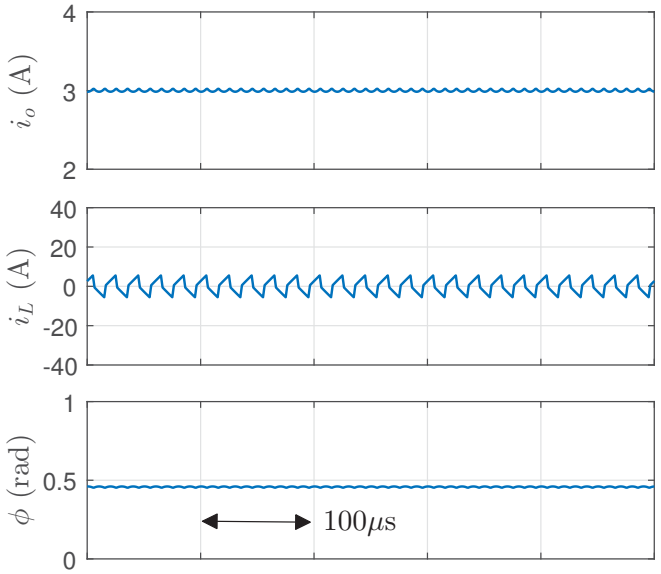

(b)

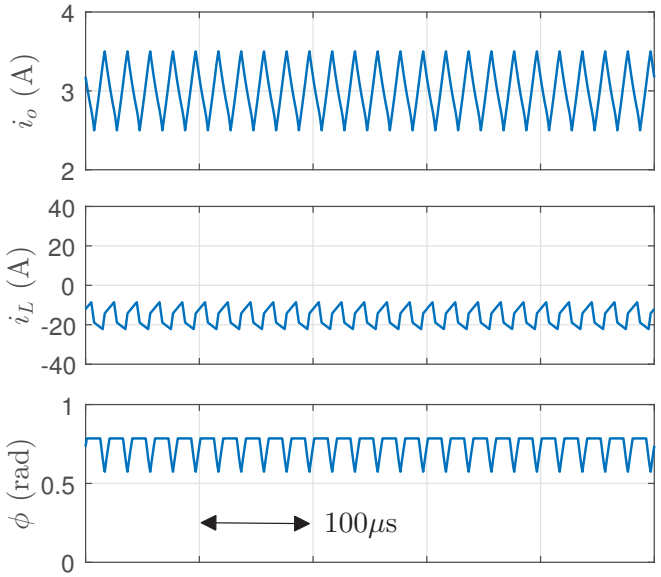

(c)

Fig. 6. Closed-loop simulation results for voltage source load with two PI controllers, (a) $k_p = 0.2$ (stable), (b) $k_p = 0.5$ (unstable).

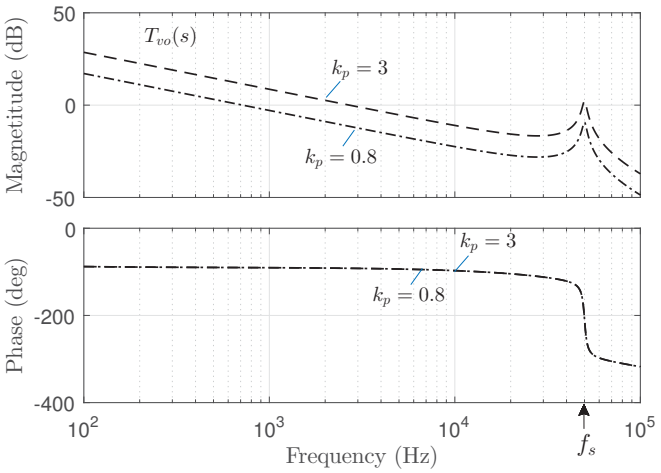

(a)

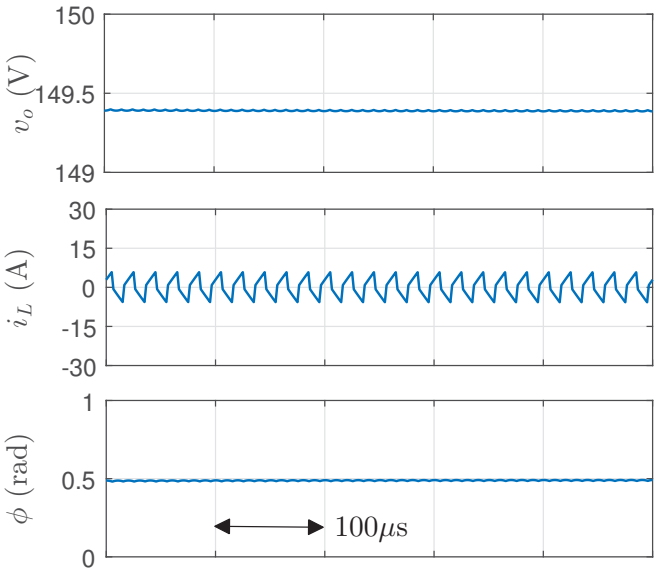

(b)

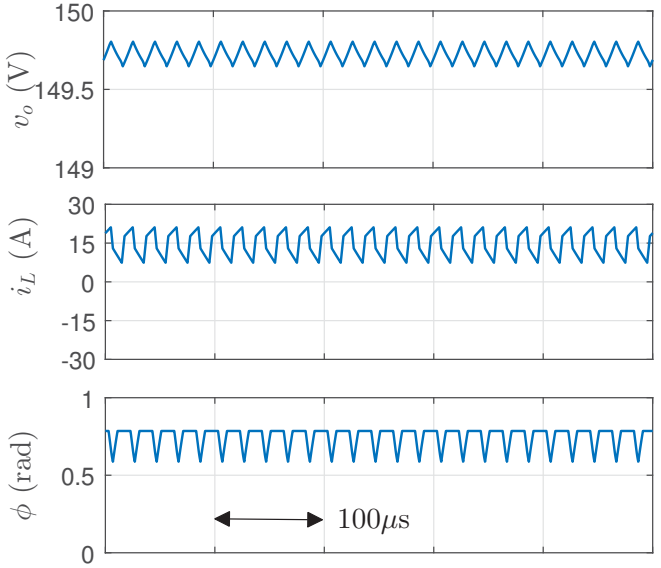

(c)

Fig. 7. Closed-loop simulation results for resistive load with two P controllers, (a) $k_p = 0.8$ (stable), (b) $k_p = 3$ (unstable).

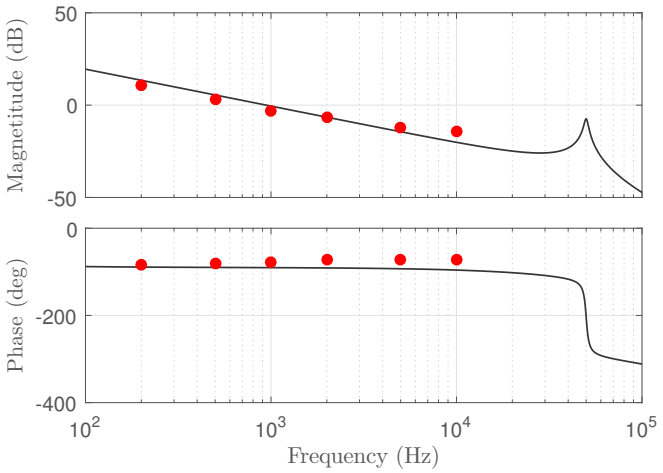

Fig. 8. Experimental result of small-signal dynamics of $G_{v_o\phi}(s)$. $V_g = 200\,\text{V}$, $R_L = 47\,\Omega$ and $P_o = 480\,\text{W}$.

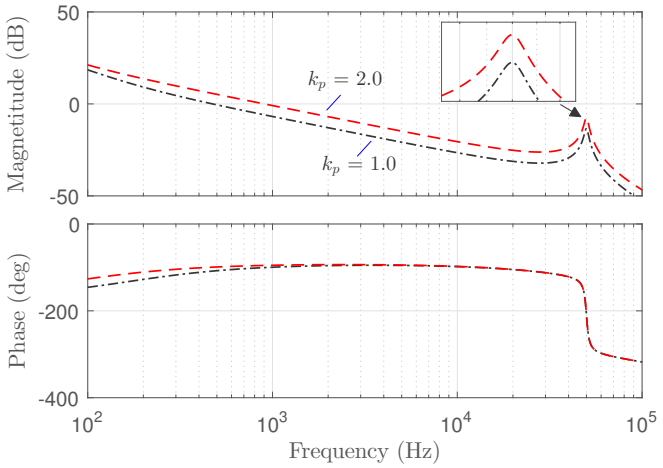

Fig. 9. Loop gains of the DAB converter with two PI controllers in experimental test.

with $k_p = 0.8$ (Fig. 7b), the DAB converter achieves stable operation. In contrast, with $k_p = 3$ (Fig. 7c), phase shift ϕ severely oscillates, therefore, the converter is unstable. These results are consistent with the analysis in section III-C and confirm that the bandwidth of DAB converters is restricted by the resonance near the switching frequency.

B. Experimental Verification

Small-signal dynamics of the DAB converter with resistive load are experimentally verified, under the condition of $V_g = 200\,\text{V}$, $R_L = 47\,\Omega$ and $P_o = 480\,\text{W}$ as shown in Fig. 8, which indicates good consistence with proposed model.

Voltage closed-loop control is experimentally performed with $V_g = 100\,\text{V}$ and $R_L = 47\,\Omega$. The reference voltage is set to $V_{ref} = 80\,\text{V}$. Two blocking capacitors are placed in both primary and secondary in series with transformer windings, which prevent transformer from saturation when the converter is unstable. Two PI controllers are respectively

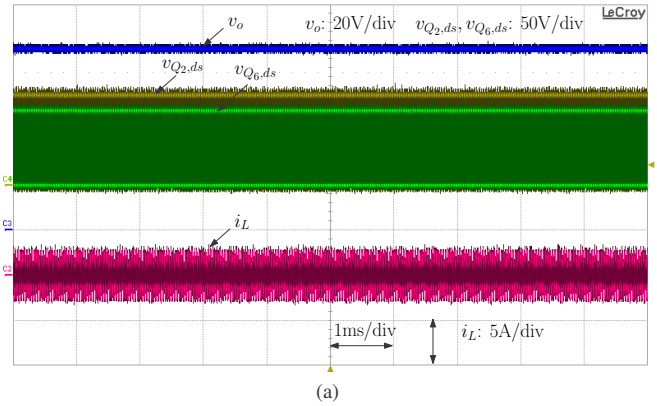

(a)

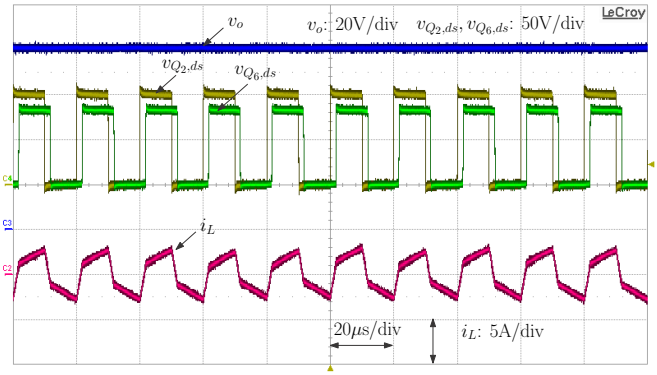

(b)

Fig. 10. Closed-loop experimental results with resistive load,$k_p = 1.0$.

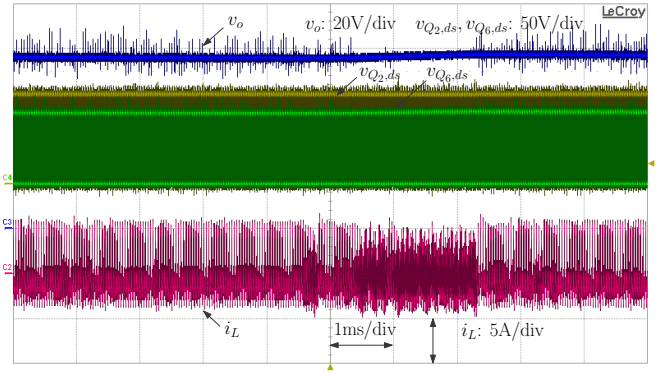

(a)

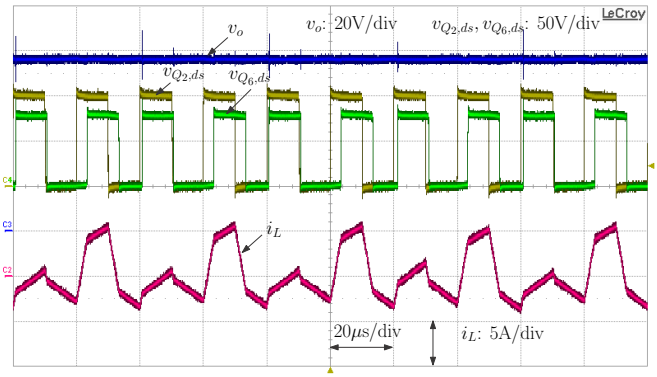

(b)

Fig. 11. Closed-loop experimental results with resistive load, $k_p = 2.0$.

employed with the same integral coefficient $k_i = 1000$ but different proportional coefficient $k_p = 1.0$ and $k_p = 2.0$. The bode plot of loop gains are reported in Fig. 9. The experimental waveforms are shown in Fig. 10 and Fig. 11. It can be seen, with $k_p = 1.0$, the converter can achieve stable operation. While with the increase of k_p, the resonant peak is close to $0\,\mathrm{dB}$ line and the magnitude margin is reduced, which leads to unstable operation, as shown in Fig 11. The experimental result is consistent with theoretical analysis and simulation, and further confirms the resonant phenomenon near switching frequency limits the bandwidth of DAB converters. In a compensator design, care should be taken at the frequency response near switching frequency, a PI controller with low gain may be needed to stabilize the control loop.

V. Conclusion

The small-signal analytical transfer functions for phase shift modulated DAB converters are derived using phasor transformation, showing significant simplification over generalized average modeling approach. Resonant phenomenon near the switching frequency is also disclosed offering meaningful guidance for closed-loop controller design. Theoretical results are verified via simulation and experiments.

References

[1] H. Qin and J. W. Kimball, "Generalized average modeling of dual active bridge dc-dc converter," IEEE Transactions on Power Electronics, vol. 27, no. 4, pp. 2078–2084, April 2012.

[2] H. Bai, C. Mi, C. Wang, and S. Gargies, "The dynamic model and hybrid phase-shift control of a dual-active-bridge converter," in 2008 34th Annual Conference of IEEE Industrial Electronics, Nov 2008, pp. 2840–2845.

[3] K. Zhang, Z. Shan, and J. Jatskevich, "Large- and small-signal average-value modeling of dual-active-bridge dc-dc converter considering power losses," IEEE Transactions on Power Electronics, vol. 32, no. 3, pp. 1964–1974, March 2017.

[4] S. R. Sanders, J. M. Noworolski, X. Z. Liu, and G. C. Verghese, "Generalized averaging method for power conversion circuits," IEEE Transactions on Power Electronics, vol. 6, no. 2, pp. 251–259, Apr 1991.

[5] C. T. Rim and G. H. Cho, "Phasor transformation and its application to the dc/ac analyses of frequency phase-controlled series resonant converters (src)," IEEE Transactions on Power Electronics, vol. 5, no. 2, pp. 201–211, Apr 1990.

[6] D. Seltzer, L. Corradini, D. Bloomquist, R. Zane, and D. Maksimovi, "Small signal phasor modeling of dual active bridge series resonant dc/dc converters with multi-angle phase shift modulation," in 2011 IEEE Energy Conversion Congress and Exposition, Sept 2011, pp. 2757–2764.

[7] Y. Yin, R. Zane, J. Glaser, and R. W. Erickson, "Small-signal analysis of frequency-controlled electronic ballasts," IEEE Transactions on Circuits and Systems I: Fundamental Theory and Applications, vol. 50, no. 8, pp. 1103–1110, Aug 2003.